Journal of Sound and Vibration (2000) **235**(1), 1–23
doi:10.1006/jsvi.1999.2913, available online at http://www.idealibrary.com on IDEAL®

SYSTEM PROPERTIES OF FLEXIBLE STRUCTURES WITH SELF-SENSING PIEZOELECTRIC TRANSDUCERS

S. Carabelli and A. Tonoli

Mechatronics Laboratory, Politecnico di Torino, Corso Duca degli Abruzzi 24, *I*-10129 *Torino, Italy*.
E-mail: *tonoli@polito.it*.

(*Received* 26 *May* 1999)

Active and passive implementations of self-sensing readout networks are studied in terms of system properties such as the poles and the zeros of their transfer functions. The location of the zeros is shown to be dependent on two non-dimensional parameters related to the balancing condition of the readout bridge and to the compensation of its losses, while it is not affected by the active or passive implementation of the readout bridge. In the case of ideal "loss compensation" a graphical procedure is employed to describe the migration of the zeros. Even if the self-sensing arrangement guarantees the colocation of the sensing and actuating functions, the graphical procedure shows the possibility of non-minimum phase zero coupls for balancing conditions close to the so-called "electrical balancing". The effects of model reduction techniques such as truncation or residualization is then studied, starting from a model of the system in terms of modal coordinates. Truncation is shown to be better suited to determine the "electrical balancing" condition while residualization gives a better approximation of the system zeros. The conditions of electrical balancing and loss compensation are then related to a condition of minimum dependance of the self-sensing bridge output from the driving electrical input. This property can be practically exploited to devise an adaptive readout bridge which can automatically reach the balancing conditions and the loss compensation or to identify the electrical parameters of the piezoelectric transducer. Experimental tests performed on a beam and a plate structures provided with self-sensing piezoelectric transducers are used to validate the analytical models.

1. INTRODUCTION

In the case of non-dissipative behaviour piezoelectric materials can be considered as transducers causing a direct and reversible energy transformation from electrical to mechanical forms. The reversibility can be exploited in the so-called self-sensing configurations with the aim of obtaining information about the mechanical states while acting upon them.

In principle, the self-sensing operation of a piezoelectric transducer can be obtained by the simultaneous measurement of the voltage and the current at its electric terminals. However, in the case when the transducer is voltage driven, part of the current flowing through is related to the mechanical states. Unfortunately, because of the highly capacitive nature of the piezoelectric transducer, this part of the current is orders of magnitude smaller than the total current. This problem can be solved by including the transducer in the measuring arm of a bridge network [1–3]. The piezoelectric transducer is connected in series with a current or a charge meter, depending on whether an output related to the structural displacements or velocities is sought, to form the measuring arm of the bridge. The reference arm twins the measuring arm except where piezoelectric interaction is

0022-460X/00/310001 + 23 $35.00/0

concerned. The measuring devices included in the bridge can be passive or active. In the first case, a simple resistor or capacitor is placed in series with the piezoelectric and reference admittances. In the second, active networks based on operational amplifiers are used [4, 5].

The accurate matching or balancing of the readout network is of great importance in order to obtain a suitable output signal. Unfortunately, even in the case of a nominally balanced bridge, the different values of the losses within its arms strongly affect the open-loop transfer function zero [6, 8].

In this paper, some aspects of the passive and active implementation of the balancing condition, and of the losses compensation of the readout bridge circuits, are analyzed and experimentally verified on beam and plate test rigs equipped with a single piezoelectric transducer.

The structural properties of the electromechanical system, including the flexible structure equipped with piezoelectric transducers connected to their power and signal conditioning electronics, is studied in terms of zeros and poles location (for an introduction to this approach see reference [9]). The operation of the piezoelectric transducer in a self-sensing configuration, i.e., as actuator and sensor at the same time, guarantees at least the mechanical colocation of the system (for the problems arising from noncolocation see, for example reference [10], for the effects of sensor and actuator dynamics [11]).

The behaviour of the self-sensing system is studied as a function of two non-dimensional parameters related to the balancing condition of the readout and to the compensation of its losses. The balancing parameter is shown to cause a migration of the zeros on the complex plane similar to that occurring in non-self-sensing and colocated systems when the sensor–actuator pairs are moved on the structure. On the other hand, the loss compensation parameter is shown to cause a substantial "damping" of the zeros. When the losses affecting the piezoelectric transducer are of resistive nature, the present analysis shows that a signal related to the mechanical states can only be obtained from the self-sensing system if both the condition of electrical balancing and loss compensation are satisfied.

The analysis developed here shows that a more general colocation condition is obtained for the electromechanical system when the so-called electrical balancing of the readout bridge is met: in this case the output of the readout bridge does not depend on the electrical drive to the transducer but only on the mechanical dynamics.

The practical achievement of the electrical balancing condition is usually a critical issue that may limit the application of self-sensing transducers. The analysis presented here shows that such a condition corresponds to a minimum of the system output when excited by random white noise, i.e., a self-tuning procedure can be used to tune the bridge using its output only.

2. ELECTROMECHANICAL MODELLING

The equation of motion of a structure including piezoelectric transducers can be formulated in terms of mechanical displacements and voltages applied to the piezoelectric electrodes [12]. Assuming the reversibility of piezoelectric interaction and the linearity of the electromechanical system for the case of a single transducer, the following dynamic equation can be written:

$$[\mathbf{M}]\{\ddot{\mathbf{x}}\} + [\mathbf{C}]\{\dot{\mathbf{x}}\} + [\mathbf{K}]\{\mathbf{x}\} + [\boldsymbol{\Theta}]v_p = \{\mathbf{F}\}, \tag{1}$$

$$-[\boldsymbol{\Theta}]^{\mathrm{T}}\{\mathbf{x}\} + C_p v_p = q_p, \tag{2}$$

where $[\mathbf{M}]$, $[\mathbf{C}]$ and $[\mathbf{K}]$ are, respectively, the mass, the damping and the short circuit stiffness matrices and C_p is the capacitance of the piezoelectric. Matrix $[\mathbf{\Theta}]$ is responsible for the electromechanical coupling between the voltage v_p acting on the piezoelectric transducer and the mechanical displacements $\{\mathbf{x}\}$. The above-mentioned matrices are usually obtained using the finite element method.

From the purely electrical point of view, each piezoelectric may be considered as a single-port device whose admittance includes the mechanical dynamics. The Laplace transform of the electric admittance $Y_p(s)$ at the electrodes of the transducer is obtained by substituting the displacement $\{\mathbf{x}\}$ obtained from equation (1) in the derivative of equation (2) (in order to deal with currents instead of charges)

$$Y_p(s) = \frac{I_p(s)}{V_p(s)} = sC_p + \frac{1}{R_{lp}} + s[\mathbf{\Theta}]^{\mathrm{T}}([\mathbf{M}]s^2 + [\mathbf{C}]s + [\mathbf{K}])^{-1}[\mathbf{\Theta}]. \tag{3}$$

The first contribution to the admittance sC_p takes the purely capacitive nature of the piezoelectric device into account as if all mechanical degrees of freedom were constrained. The resistance R_{lp} is added in parallel to the piezoelectric capacitance to model the losses within the device. Conversely, for the unconstrained and voltage-driven system, the measure of the current includes the information about the mechanical velocities giving way to the last term of equation (3).

Remark 1. To account for the hysteretic nature of the piezoelectric, the piezoelectric capacitance may be modelled with a complex term analogous to the standard mechanical representation of structural damping [6]. The use of a simple resistance in parallel with an ideal capacitance to model the losses within the piezoelectric allows indications to be drawn on an analytical basis and is acceptable when operating in a limited frequency range.

Due to the usually small contribution given by the mechanical term to the admittance (3), the contribution $sC_p + 1/R_{lp}$ to the voltage to current response must be physically cancelled as closely as possible to obtain an admittance primarily related to the mechanical dynamics. This is usually obtained by including the piezoelectric transducer into a bridge readout circuit [1, 2, 13]. The reference arm of the bridge must replicate as closely as possible the purely electrical behaviour of the piezoelectric device, i.e.,

$$Y_r(s) = sC_r + \frac{1}{R_{lr}} \tag{4}$$

in its basic version. The choice of the reference capacitance C_r is usually involved in the so-called *balancing procedure* while that of reference loss resistance R_{lr} is involved in the so-called *loss compensation procedure*. Together, the two procedures allow the effective self-sensing operation of the piezoelectric transducer to be obtained.

2.1. PASSIVE READOUT BRIDGE

In the readout bridge, the current-measuring devices connected in series with a piezoelectric transducer and the reference capacitor are usually implemented with shunt resistors as in Figure 1. The transfer function from the input driving voltage $V_{in}(s)$ to the differential output $V_{out}(s)$ is the following:

$$\frac{V_{out}(s)}{V_{in}(s)} = H_{pass}(s) = \frac{R_r Y_r(s) - R_p Y_p(s)}{(1 + R_r Y_r(s))(1 + R_p Y_p(s))}. \tag{5}$$

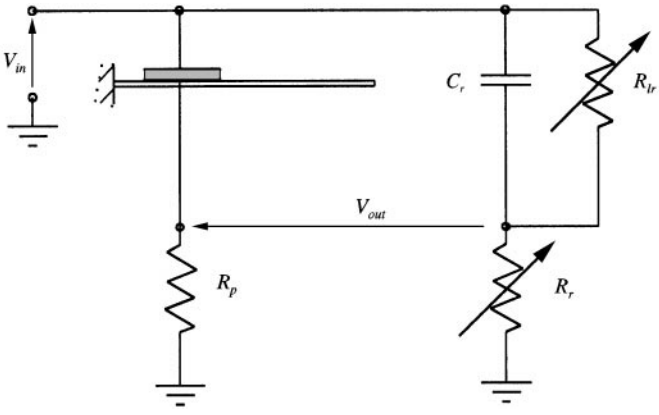

Figure 1. Piezoelectric self-sensing configuration: passive readout bridge.

Taking the admittances $Y_p(s)$ (3) and $Y_r(s)$ (4) into account,

$$\frac{V_{out}(s)}{V_{in}(s)} = \frac{[s(R_rC_r - R_pC_p) + (R_p/R_{lp} - R_r/R_{lr})] - sR_p(n(s)/d(s))}{(1 + R_r/R_{lr} + sR_rC_r)(1 + R_p/R_{lp} + sR_pC_p + sR_p(n(s)/d(s)))}$$

$$= \frac{[s(R_rC_r - R_pC_p) + (R_p/R_{lp} - R_r/R_{lr})]d(s) - sR_pn(s)}{(1 + R_r/R_{lr} + sR_rC_r)((1 + R_p/R_{lp} + sR_pC_p)d(s) + sR_pn(s))}, \tag{6}$$

where

$$\frac{n(s)}{d(s)} = [\mathbf{\Theta}]^{\mathrm{T}}([\mathbf{M}]s^2 + [\mathbf{C}]s + [\mathbf{K}])^{-1}[\mathbf{\Theta}] \tag{7}$$

is the mechanical contribution to the electrical admittance due to the piezoelectric interaction. The presence of the shunt resistors induces two dynamics in addition to the mechanical one: a purely electrical dynamic due to the reference arm and an electromechanically coupled dynamic due to the measuring arm of the bridge.

In order to cancel out the first contribution to the numerator of equation (6), the standard balancing condition and loss compensation for the readout bridge are assumed to be

$$R_rC_r = R_pC_p, \qquad \frac{R_p}{R_{lp}} = \frac{R_r}{R_{lr}} \tag{8, 9}$$

which simplifies equation (6) to

$$\frac{V_{out}(s)}{V_{in}(s)} = \frac{-sR_pn(s)}{(1 + R_r/R_{lr} + sR_rC_r)((1 + R_p/R_{lp} + sR_pC_p)d(s) + sR_pn(s))}. \tag{10}$$

It should be noted that the zero pattern of the transfer function of the balanced bridge is reduced to that of the mechanical contribution (7) to the piezoelectric admittance (3).

2.2. ACTIVE READOUT BRIDGE

In order to improve the measurement of the current, an alternative solution is to substitute the shunt resistors with active current to voltage converters (Figure 2). In the

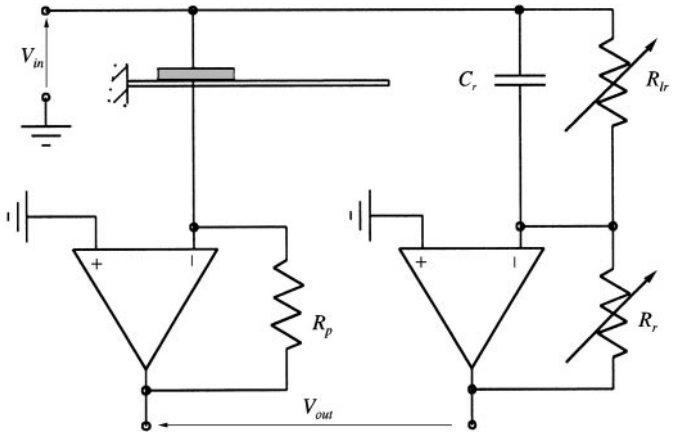

Figure 2. Piezoelectric self-sensing configuration: active readout bridge.

electromechanical frequency range, the operational amplifiers can be assumed to be almost ideal and the output transfer function of the bridge simplifies to the following:

$$\frac{V_{out}(s)}{V_{in}(s)} = H_{act}(s) = R_r Y_r(s) - R_p Y_p(s) \tag{11}$$

and consequently

$$\begin{aligned}\frac{V_{out}(s)}{V_{in}(s)} &= \left[s(R_r C_r - R_p C_p) + \left(\frac{R_p}{R_{lp}} - \frac{R_r}{R_{lr}} \right) \right] - sR_p \frac{n(s)}{d(s)} \\ &= \frac{[s(R_r C_r - R_p C_p) + (R_p/R_{lp} - R_r/R_{lr})]\, d(s) - sR_p n(s)}{d(s)}.\end{aligned} \tag{12}$$

Comparison of equations (6) and (12) shows that the active bridge solution does not change the zeros pattern but reduces the poles pattern to the purely mechanical one.

Under the aforementioned standard balancing and compensation conditions (8) and (9), equation (12) reduces to

$$\frac{V_{out}(s)}{V_{in}(s)} = \frac{-sR_p n(s)}{d(s)} \tag{13}$$

whose overall dynamics do not show any dependence from the readout bridge, at least as long as the ideal behaviour of the operational amplifiers may be, practically, assumed. Note that the ideality assumption for the operational amplifier leads to a improper transfer function, as in the case of an ideal derivative action where the causality poles are out of the frequency range of interest.

3. STRUCTURAL PROPERTIES

In the following, the structural properties of a flexible structure with self-sensing piezoelectric transducers are studied in terms of poles and zeros patterns. The analysis is performed in the cases of passive and active readout bridge configurations to illustrate their

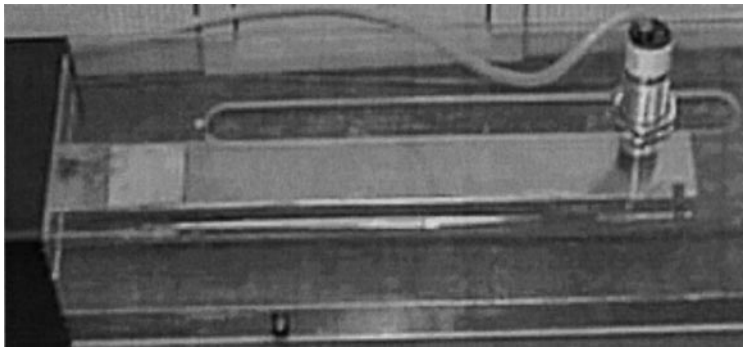

Figure 3. Beam test rig (the position sensor at the beam tip is used for comparison only).

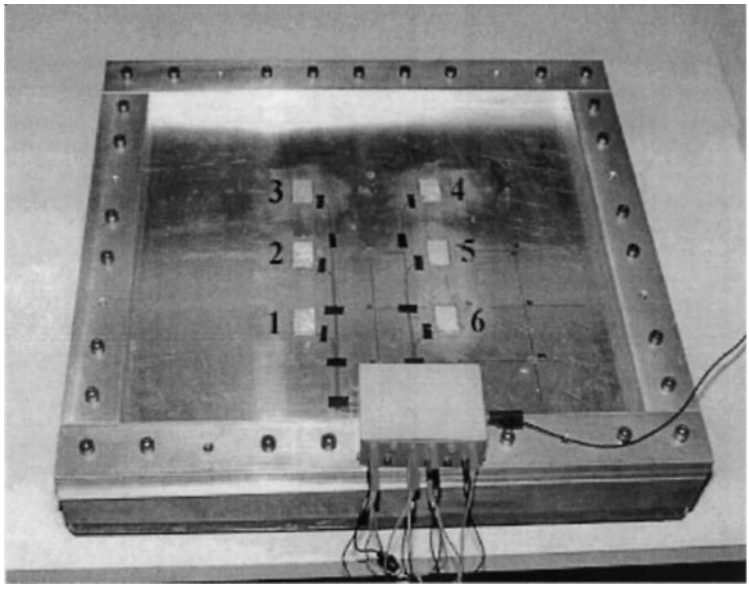

Figure 4. Plate test rig.

peculiarities. The kind of bridge configuration and its balancing condition are usually to be chosen as design parameters.

The examples reported in the following are related to the experimental test rigs (see Figures 3 and 4) described in Appendix A when not otherwise indicated.

3.1. POLE STRUCTURE

As the readout bridge is made of two arms in parallel, from equation (6) the poles of the passive bridge are distinguished in two decoupled sets: a purely electrical one due to the reference arm of the bridge

$$\left(1 + \frac{R_r}{R_{lr}} + sR_rC_r\right) = 0 \tag{14}$$

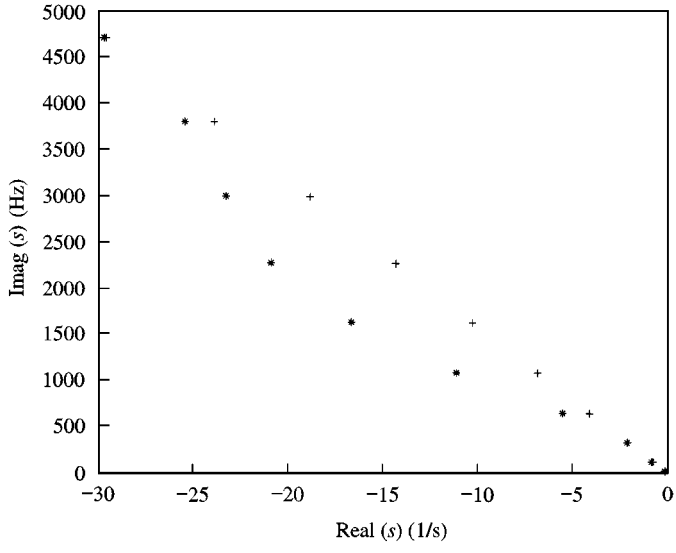

Figure 5. Poles of system (beam structure) transfer function with passive readout bridge: short circuit (+) versus $R_p = 10\,\mathrm{k}\Omega$ (*)

and an electromechanical one due to the piezoelectric arm of the bridge that shows a coupling between the electrical and mechanical dynamics

$$\left(1 + \frac{R_p}{R_{lp}} + sR_pC_p\right)d(s) + sR_pn(s) = 0. \tag{15}$$

Nevertheless, the contribution of the second term in equation (15) is usually negligible and results in a slight increase of the real part of the poles of the mechanical structure with short-circuited piezoelectric ($R_p = 0$). With reference to Figure 5, it is to be noted that the natural frequencies of the system are only marginally affected (1–2%) because of the light damping of the structure (model damping $< 0{\cdot}001$) and the small values of piezoelectric interaction ($[\boldsymbol{\Theta}]$ matrix).

In the case of an active bridge, it follows from equation (12) that the poles of the system are not affected by the readout circuit. In this case, the underlying assumption is the ideality of the operational amplifier in the bandwidth of interest.

3.2. ZERO STRUCTURE

In the following, the dependence of the zeros of the system is studied as a function of the bridge electrical parameters. By comparison of equations (6) and (12), the zeros of the transfer function of the piezoelectric transducer do not depend on the kind of the readout circuit and are given by

$$\left[s(R_rC_r - R_pC_p) + \left(\frac{R_p}{R_{lp}} - \frac{R_r}{R_{lr}}\right)\right] - sR_p\frac{n(s)}{d(s)}$$

$$= sR_pC_p\beta + \eta - sR_p\frac{n(s)}{d(s)} = 0, \tag{16}$$

where the dimensionless balancing parameter β and loss compensation parameter η are defined as

$$\beta = \frac{R_r C_r}{R_p C_p} - 1, \qquad \eta = \frac{R_p}{R_{lp}} - \frac{R_r}{R_{lr}} \tag{17, 18}$$

when modal co-ordinates are adopted as mechanical degrees of freedom, the mechanical contribution of equation (7) becomes

$$\frac{n(s)}{d(s)} = \sum_{i=1}^{\infty} \frac{\theta_i^2}{(s^2 + 2\zeta_i \omega_i s + \omega_i^2)}, \tag{19}$$

where θ_i, ζ_i and ω_i are the ith modal electromechanical coupling, damping ratio and natural frequency respectively. The quadratic form for the modal electromechanical coupling terms is due to the colocation of sensor and actuator functions.

The substitution of equation (19) into equation (16) leads to the following expression for the zero equation:

$$sR_p C_p \beta + \eta = sR_p \sum_{i=1}^{\infty} \frac{\theta_i^2}{(s^2 + 2\zeta_i \omega_i s + \omega_i^2)}. \tag{20}$$

The system zeros are the intersections of the two following functions on the complex s plane:

$$H_1(s) = sR_p C_p \beta + \eta, \qquad H_2(s) = sR_p \sum_{i=1}^{\infty} \frac{\theta_i^2}{(s^2 + 2\zeta_i \omega_i s + \omega_i^2)}. \tag{21}$$

In order to simplify the analysis and to give a straightforward graphical interpretation of the dependence of the zeros from the balancing parameter β, the following assumptions are made:

- no modal damping ($\zeta_i = 0$),
- ideal loss compensation ($\eta = 0$).

With these assumptions, equation (20) can be simplified into a biquadratic form of s and its solutions can be assumed either as $s = \pm \mathrm{i}\omega_z$ or as $s = \pm \omega_z$ with $\omega_z \in \mathscr{R}^+$.

1. In the case of $s = \pm \mathrm{j}\omega_z$, the zeros are imaginary and conjugate given by

$$\beta = \frac{1}{C_p} \sum_{i=1}^{\infty} \frac{\theta_i^2}{(-\omega_z^2 + \omega_i^2)}, \tag{22}$$

where the left-hand term is a constant depending on the balancing parameter β and the right-hand term is the superposition of all modal contributions, as shown in Figure 6. Since the all residuals θ_i^2/ω_i^2 are positive, the right-hand term function intersects the ω-axis giving way to an interlaced pattern with the natural frequencies. Depending on the value of balancing parameter β, three different type of intersections are found:

(a) for $-\infty < \beta < 0_-$ each zero pair follows a pole couple $\pm \mathrm{j}\omega_i$ (the zero-pole alternating pattern begins with a pole couple),
(b) for $0_+ < \beta < \beta^* = (1/C_p) \sum_{i=1}^{\infty} \theta_i^2/\omega_i^2$ each zero couple follows a pole couple $\pm \mathrm{j}\omega_i$ (the zero-pole alternating pattern begins with a pole couple) but the last,
(c) for $\beta^* < \beta < +\infty$ each zero couple precedes a pole couple $\pm \mathrm{j}\omega_i$ (the zero-pole alternating pattern begins with a zero couple).

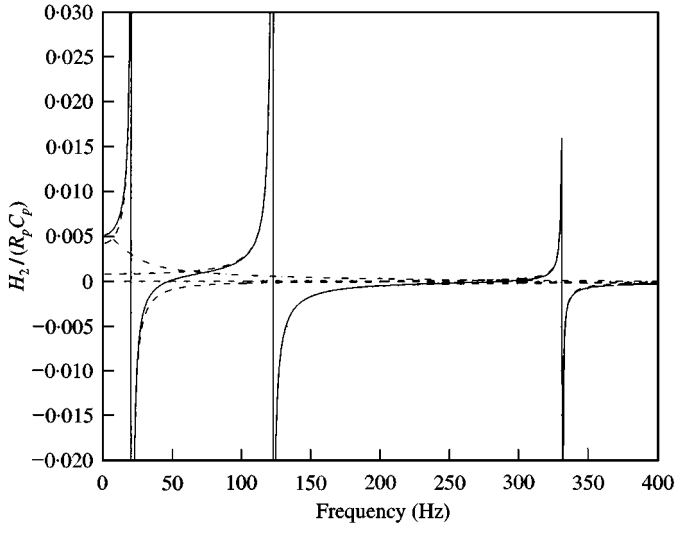

Figure 6. Graphical interpretation of the system zeros. The complex and conjugate zeros are found as intersections between horizontal lines (corresponding to different values of the balancing parameter β) and the curve (continuous line) relative to the superposition of modal contributions (dashed lines), i.e., second term of equations (22). The real and opposite couple of zeros is found as intersection of the horizontal β line and the curve (dot-dashed line) relative to the second term of equation (23).

2. In the case of $s = \pm \omega_z$, the zeros are real and opposite and given by

$$\beta = \frac{1}{C_p} \sum_{i=1}^{\infty} \frac{\theta_i^2}{(\omega_z^2 + \omega_i^2)}, \tag{23}$$

the right-hand term is represented by the dot-dashed line of Figure 6. The intersection occurs only for $0_+ < \beta < \beta^*$.

The overall root locus of the zeros depending on the balancing parameter β is shown in Figure 7. For β increasing from $-\infty$, the zeros are shown to migrate on the imaginary axis towards, higher frequencies. For the case of electrical balancing condition ($\beta = 0$), the last pair of zeros goes to infinity to re-appear on the real axis to reach the origin for $\beta = \beta^*$. For a further increase of β, the two real and opposite zeros move again on the imaginary axis tending to the couple of complex conjugate poles of lowest frequency. The other couples of complex conjugate zeros tend to the "following" couple of poles.

Although the reference to the "last couple of zeros" is correct only in the case of a discrete (or discretized) mechanical system, it has been taken as valid also in the case of a continuous system, characterized by an infinite number of resonant frequencies. The migration on the real axis of the "last couple of zeros" is needed in this case to preserve the relative order between numerator and denominator of the system transfer function.

The zeros natural frequency as an explicit function of the balancing parameter β are reported in Figure 8. This diagram has been obtained by standard numerical computation from the state-space model of the system and should be compared with the same results obtained with the graphical procedure shown in Figure 6.

Remark 2. The geometrical colocation of sensors and actuators intrinsic in the self-sensing configuration of the piezoelectric transducer leads to a zero pattern that depends only on the balancing of the readout bridge, i.e., on a purely electrical condition. Note that a couple of real and opposite zeros are to be expected for β greater than zero.

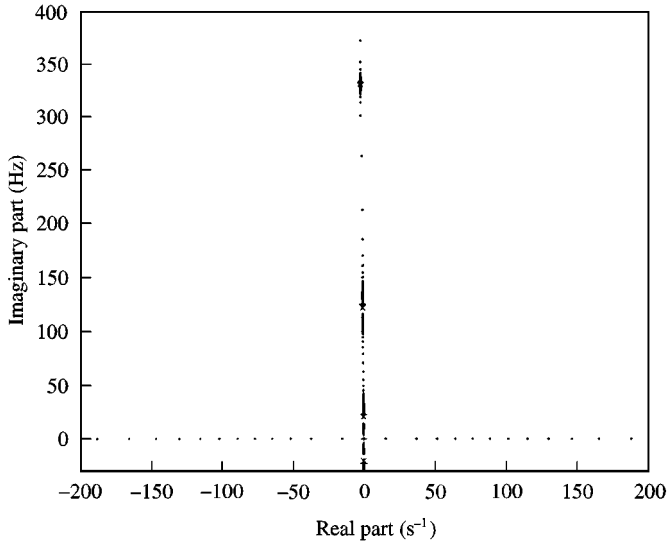

Figure 7. Zeros locus as a function of balancing parameter β in the case of $\eta = 0$. (+) indicate zeros under electrical balancing condition and (*) indicate poles.

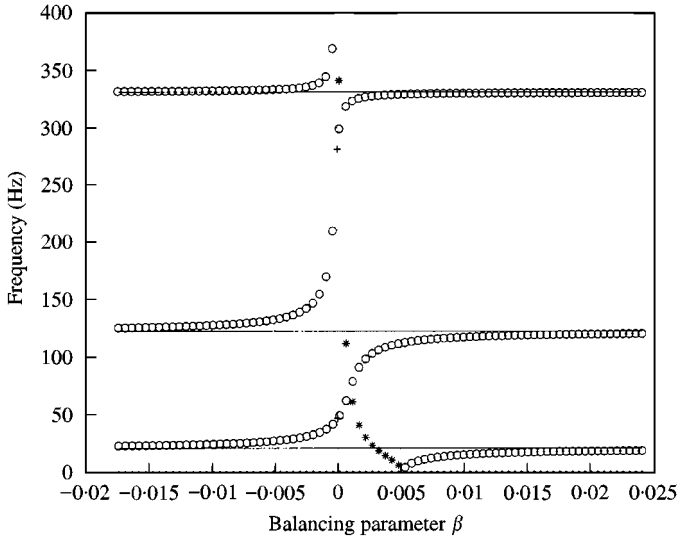

Figure 8. Zeros diagram as a function of balancing parameter β in the case of $\eta = 0$. (○) indicate complex and conjugate zeros, (*) real and opposite zeros, and (+) zeros under electrical balancing condition. Continuous lines indicate poles.

The balancing condition $\beta = \beta^*$ can be physically characterized using a modal co-ordinate transformation for the admittance of the piezoelectric of equation (3):

$$Y_p(s) = sC_p + \frac{1}{R_{lp}} + s\sum_{i=1}^{\infty} \frac{\theta_i^2}{(s^2 + 2\zeta_i\omega_i s + \omega_i^2)}. \tag{24}$$

Taking the mechanical term into account, the overall capacitance of the piezoelectric is

$$C_p^* = C_p + \sum_{i=1}^{\infty} \frac{\theta_i^2}{\omega_i^2}. \tag{25}$$

This is the value that can be measured with an impedance meter when the piezoelectric transducer is installed on a mechanical structure. From the definition of the balancing parameter β given in equation (17), condition $\beta = \beta^*$ implies

$$R_p C_p^* = R_r C_r, \tag{26}$$

i.e. the bridge is balanced using C_p^* instead of C_p as capacitance of the piezoelectric transducer.

The substantial difference shown in Figure 6 between the zero pattern for $\beta = 0$ and $\beta/$ indicates that the mechanical contribution to the piezoelectric capacitance must be eliminated to determine the electrical balancing condition.

A further physical insight into the significance of the electrical balancing condition $\beta = 0$ may be reached as follows: in the case of the active bridge and taking the ideality of the operational amplifier into account, the voltage on the piezoelectric V_p is equal to the input voltage V_{in} and the actuator and sensor equations (1) and (2) can be written as

$$(s^2[\mathbf{M}] + s[\mathbf{C}] + [\mathbf{K}])\{\mathbf{X}(s)\} = -[\mathbf{\Theta}]V_{in}(s), \tag{27}$$

$$-s[\mathbf{\Theta}]^{\mathrm{T}}\{\mathbf{X}(s)\} + sC_p V_{in}(s) = I_p(s). \tag{28}$$

Together with the corresponding equation for the reference arm

$$sC_r V_{in}(s) = I_r(s) \tag{29}$$

and taking the electrical losses into account, the bridge output becomes

$$V_{out}(s) = \left[s(R_r C_r - R_p C_p) + \left(\frac{R_p}{R_{lp}} - \frac{R_r}{R_{lr}} \right) \right] V_{in}(s) + sR_p[\mathbf{\Theta}]^{\mathrm{T}}\{\mathbf{X}(s)\}. \tag{30}$$

In the case of electrical balancing condition and ideal loss compensation the output is purely dependent of the mechanical states (velocities):

$$V_{out}(s) = sR_p[\mathbf{\Theta}]^{\mathrm{T}}\{\mathbf{X}(s)\}. \tag{31}$$

In this case, the input and output influence matrices of equations (27) and (31) depend on the piezoelectric coupling matrix $[\mathbf{\Theta}]$ and satisfy the condition of colocation one being the transpose of the other, apart from a proportional term R_p.

Remark 3. The migration of zeros is well known to be dependent on the absolute and relative position of actuator and sensor. In the case of colocated actuator and sensor pairs, zero couples are guaranteed to be interlaced with pole couples, i.e., moving the actuator and sensor pair on the structure causes the zero couples to migrate between the pole couples. In the case of non-colocated actuator and sensor pair, the relative position of actuator and sensor may cause the migration of the zero couples across the pole couples, i.e., the interlacing property is no longer guaranteed and several zero imaginary and conjugate couples may move on the real axis. In the present case of a self-sensing piezoelectric transducer, the interlacing property is always respected but the zero couple at the highest frequency (whichever dimension is chosen for the model) can become real depending on the

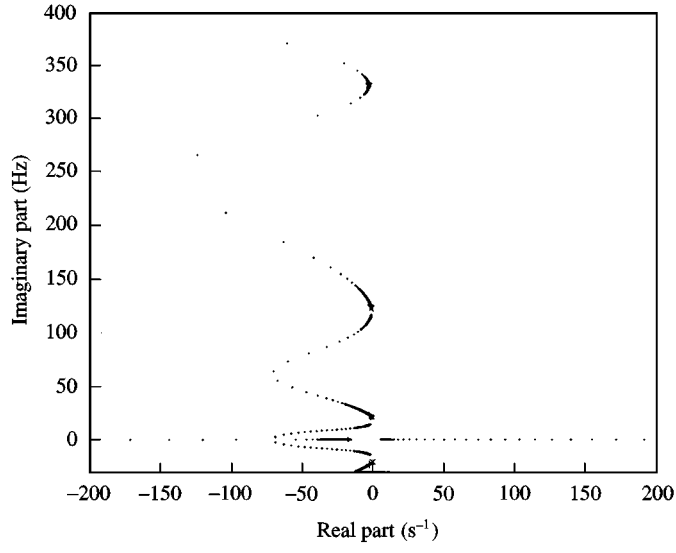

Figure 9. Zeros locus as a function of balancing parameter β in the case of $\eta \cong 0{\cdot}12$. (+) indicate zeros under electrical balancing condition and (*) indicate poles.

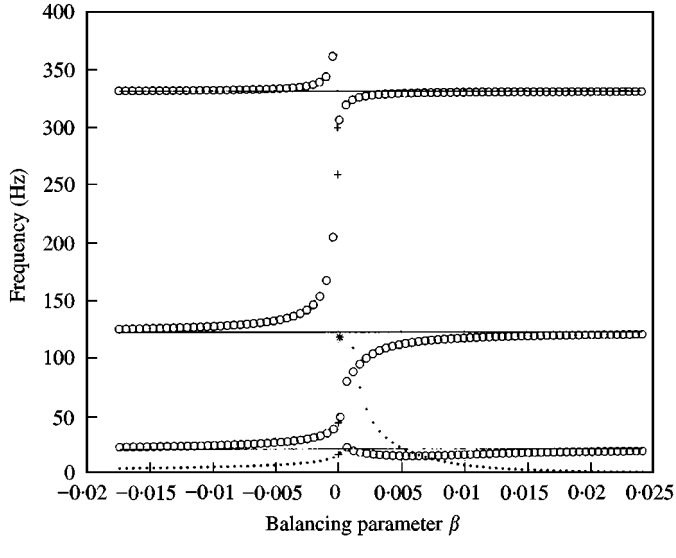

Figure 10. Zeros diagram as a functions of balancing parameter β in the case of $\eta \cong 0{\cdot}12$. (○) indicate complex and conjugate zeros, (*) real and opposite zeros, and (+) zeros under electrical balancing condition. Continuous lines indicate poles.

balancing condition. The reappearance of this zero couple on the imaginary axis is responsible for an interlaced condition with zeros at a frequency lower than that of the first pole couple.

The presence of non-compensated electrical losses in the readout bridge deeply influence the zero pattern of the system. The zero couples no longer move on the real or imaginary axes and their relative damping may become large compared with that of the mechanical structure. Figures 9 and 10 show the aforementioned behaviour even for a slight

miscompensation of the losses ($\eta \cong 0{\cdot}12$). The presence of low mechanical damping, as normally assumed for flexible structures, does not substantially change the picture relative to the ideal case.

4. EFFECTS OF MODEL REDUCTION TECHNIQUES

In order to reduce the size of the mechanical model, the contribution of the modes included in the function $H_2(s)$ of equation (21) can be split in two subsets. A first subset includes the n_r modes of lower frequency to be retained in the reduction procedure, and a second subset includes all the neglected modes:

$$H_2(s) = H_{2r}(s) + H_{2n}(s) = R_p \left(\sum_{i=1}^{n_r} \frac{\theta_i^2}{(s^2 + 2\zeta_i\omega_i s + \omega_i^2)} + \sum_{i=n_r+1}^{\infty} \frac{\theta_i^2}{(s^2 + 2\zeta_i\omega_i s + \omega_i^2)} \right). \quad (32)$$

Truncation is equivalent to the assumption that the high order modes do not contribute to the system response. This leads to the following approximation:

$$H_2(s) \cong H_{2r}(s) = R_p \sum_{i=1}^{n_r} \frac{\theta_i^2}{(s^2 + 2\zeta_i\omega_i s + \omega_i^2)}. \quad (33)$$

If the system is undamped and with ideal loss compensation, the zero structure of the reduced model can be obtained following the same graphical procedure illustrated for the complete model. When $\beta \to 0_-$, the last couple of complex conjugate zeros tend to infinity on the imaginary axis. This couple then reappears on the real axis as soon as β becomes positive.

A further increment of the parameter β lets the couple of real and opposite zeros converge to the origin for a balancing parameter β_r^* smaller than that of the complete model

$$\beta_r^* = \frac{1}{C_p} \sum_{i=1}^{n_r} \frac{\theta_i^2}{\omega_i^2} < \beta^*. \quad (34)$$

If the migration of the last couple of zeros from the imaginary axis to the real axis at infinite frequency is taken as typical of electrical balancing conditions, it follows that truncation is a reduction procedure suitable to study the balancing of a self-sensing readout bridge circuit. The condition of electrical balancing of the truncated and the complete models are in fact the same.

Remark 4. As truncation does not take the contribution at low frequency of the high order mode into account, function $H_{2r}(s)$ can be significantly different than function H_2(s). Model reduction by truncation may then be inaccurate for what the evaluation of all couples of zeros (but the last) is concerned.

To take the contribution of the high order modes into account, residualization assumes that these modes give a static response. Function $H_2(s)$ is then approximated as follows:

$$H_2(s) \cong H_{2r}(s) + H_{2n}(s = 0) = R_p \left(\sum_{i=1}^{n_r} \frac{\theta_i^2}{(s^2 + 2\zeta_i\omega_i s + \omega_i^2)} + \sum_{i=n_r+1}^{\infty} \frac{\theta_i^2}{\omega_i^2} \right). \quad (35)$$

The error involved in the approximation of function $H_2(s)$ by equation (35) is usually small in the frequency range of interest ($\omega < \omega_{nr}$), and the residualization allows an

approximation of the system zeros to be obtained better than that obtained from truncation (equation (33)).

Due to the presence of a constant term in equation (35), the last couple of complex conjugate zeros go to infinity on the imaginary axis for a not null value of the balancing parameter (β_t):

$$\beta_t = \frac{1}{C_p} \sum_{i=n_r+1}^{\infty} \frac{\theta_i^2}{\omega_i^2} > 0. \tag{36}$$

The residualized model is then electrically balanced for

$$\beta = \beta_t > 0. \tag{37}$$

Since all contributions θ_i^2/ω_i (residuals) are real and positive, β_t is between the condition of electrical balancing of the complete model and the condition of balancing $\beta = \beta^*$ that takes the piezoelectric capacitance of equation (25) into account:

$$0 < \beta_t < \beta^*. \tag{38}$$

Starting from β_t and increasing the balancing parameter β, the last couple of zeros of the reduced system appear again on the real axis. From this point on the migration of the zeros as a function of the balancing parameter follows that of the complete system.

Remark 5. From the above considerations it follows that residualization is not well suited to determine the electrical balancing condition and the range of the balancing parameter where real and opposite zeros can be found.

5. EXPERIMENTAL RESULTS

In order to validate the electromechanical model of a flexible structure with piezoelectric transducers (section 2) and its structural properties (section 3), experimental tests have been performed on the beam and the plate structures whose main characteristics are reported in Appendix A.

The first objective of the experiments was to verify the model accuracy after its reduction (equation (25) and section 4). In particular, the measured value of the piezoelectric capacitance (Figure 11) includes the mechanical contribution. The latter can be obtained from the model and its value must be subtracted from the measured capacitance C_p^* to obtain the piezoelectric electrical capacitance C_p to be used to balance the bridge according to the condition of equation (8). Note that the condition of equation (26) corresponds to the reappearance of the zeros on the imaginary axis as shown in Figure 8.

Figure 12–14 compare model and experimental transfer functions for the first and second mode of the beam and the fourth mode of the plate. Note that the readout bridge has been electrically balanced in the frequency range of the corresponding modes, i.e., equations (24) and (35) have been evaluated about the modal frequencies.

Note that the correspondence of the experimental results with the analytic models is obtained without the need of the fine tuning of the model parameters. This enables the experimental to analytic correspondence to be extended seamlessly for the phenomena related to the zeros migration (section 3.2), as graphically shown in Figures 15 and 16, and numerically in Tables 1 and 2.

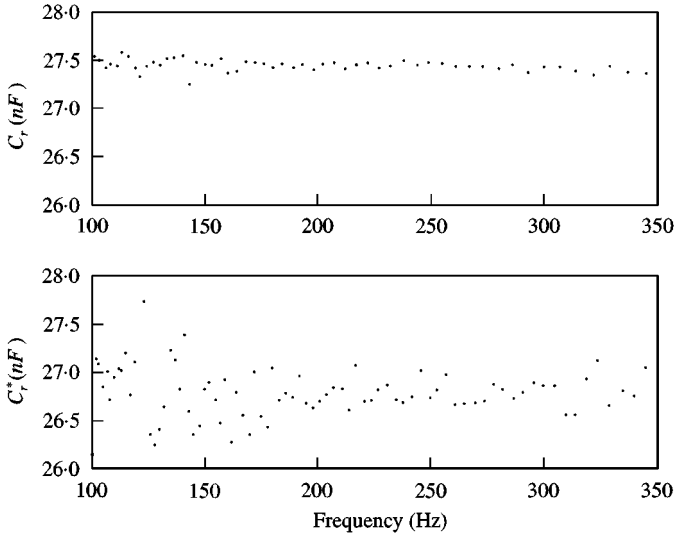

Figure 11. Measured values of capacitances C_r (mean 27·45 nF, standard deviation 0·05 nF) and C_p^* (mean 26.79 nF, standard deviation 0·37 nF). From the FE model, the mechanical contribution to C_p^* amounts to 0.65 nF.

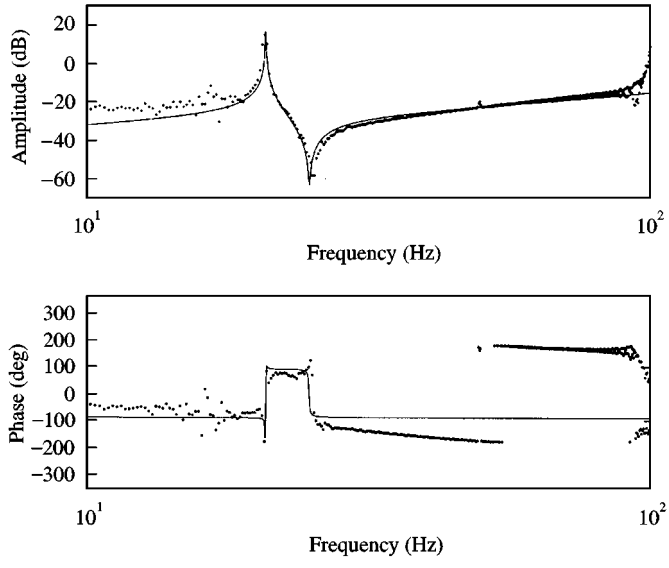

Figure 12. First mode of beam structure: model (continuous line) and measured (dots) transfer functions with electrically balanced active readout bridge.

6. EQUIVALENT ELECTRICAL BALANCING CONDITIONS

The electrical balancing condition together with the loss compensation are essential to achieve the ideal colocation of the system and its related system properties, for instance in terms of stability of the controlled structure (interlacing property and passivity). In the following, the electrical balancing and loss compensation are related to a condition of minimum dependence of the self-sensing bridge output on the driving electrical input, i.e., the output is proportional to the mechanical velocities only. This property can be

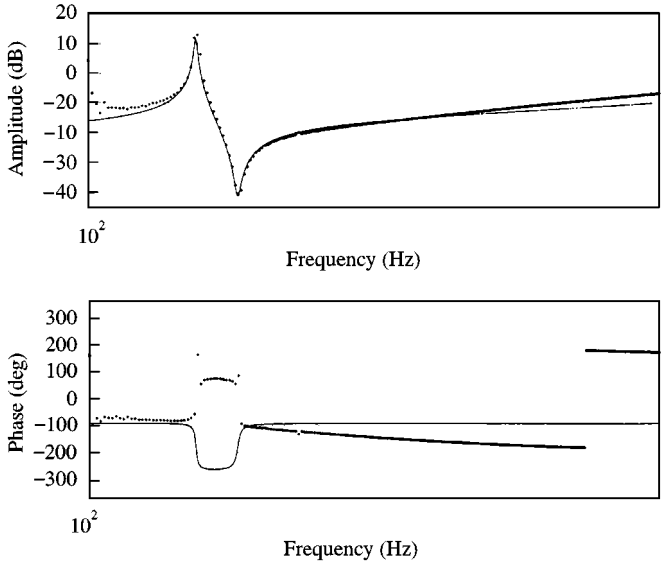

Figure 13. Second mode of beam structure: model (continuous line) and measured (dots) transfer functions with electrically balanced active readout bridge.

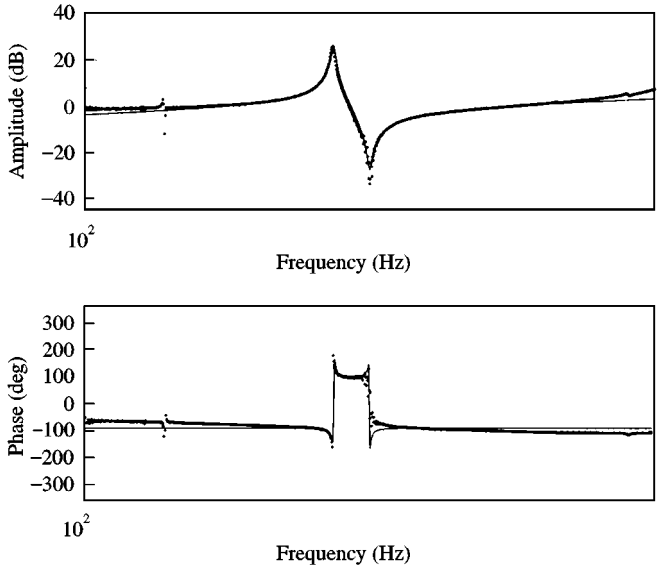

Figure 14. Fourth mode of plate structure: model (continuous line) and measured (dots) transfer functions with electrically balanced active readout bridge.

practically exploited to tune the readout bridge to achieve electrical balancing and loss compensation or, equivalently, to identify the electrical parameters of the piezoelectric transducer.

The second order norm of the output voltage signal V_{out},

$$\| V_{out}(t) \|_2 = \left(\int_0^\infty V_{out}^2(t)\, \mathrm{d}t \right)^{1/2}$$

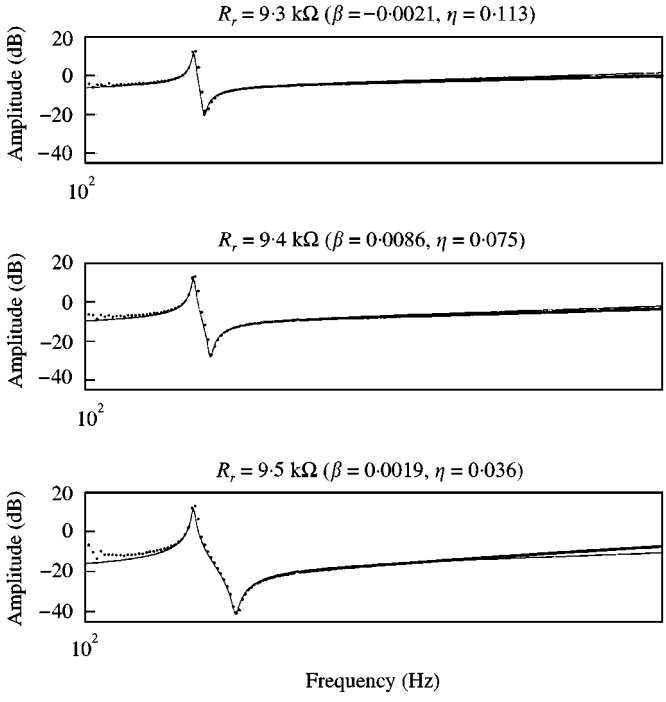

Figure 15. Zero migration near second mode of beam structure: model (continuous line) and measured (dots) transfer functions.

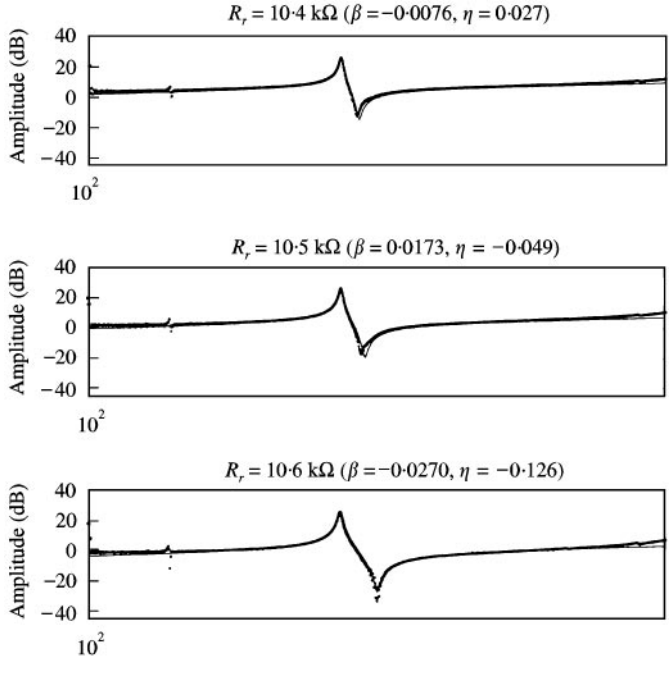

Figure 16. Zero migration near fourth mode of plate structure: model (continuous line) and measured (dots) transfer functions.

TABLE 1

Zero migration near second mode of beam structure: model versus experimental values

Balancing condition			Zero frequencies		Relative error
R_r (kΩ)	β	η	f_n(Hz)	$f_{n,exp}$(Hz)	(%)
9·3	− 0·0276	0·491	126·0	125·6	0·3
9·4	− 0·0171	0·414	127·3	127·2	0·1
9·5	− 0·0067	0·338	133·6	133·6	0·0
9·7	0·0143	0·184	117·5	116·4	0·9

TABLE 2

Zero migration near fourth mode of plate structure: model versus experimental values

Balancing condition			Zero frequencies		Relative error
R_r (kΩ)	β	η	f_n(Hz)	$f_{n,exp}$(Hz)	(%)
10·3	− 0·0021	0·1044	166·3	166·4	0·1
10·4	0·0076	0·0275	167·2	167·5	0·2
10·5	0·0173	− 0·0494	169·4	169·4	0·0
10·6	0·0270	− 0·1263	173·7	173·5	0·1
10·7	0·0367	− 0·2032	186·3	190·5	2·2

$$= \left(\frac{1}{2\pi} \int_{-\infty}^{\infty} |V_{out}(\mathrm{j}\omega)|^2 \, \mathrm{d}\omega \right)^{1/2}$$

$$= \left(\frac{1}{2\pi} \int_{-\infty}^{\infty} S_{in}(\omega) |H_{act}(\mathrm{j}\omega)|^2 \, \mathrm{d}\omega \right)^{1/2} \tag{39}$$

is to be minimized when the system (equation (11) is derived by a band-limited signal with a power spectral density $S_{in}(\omega)$ given by

$$S_{in}(\omega) = 1 \quad \text{for } \omega \in (-\omega_{max}, \omega_{max}), \tag{40}$$

$$S_{in}(\omega) = 0 \quad \text{otherwise},$$

i.e., the following minimization problem is assumed:

$$\min_{\beta,\eta} \| V_{out}(\omega_{max}; \beta, \eta) \|_2 = \min_{\beta,\eta} \left(\frac{1}{2\pi} \int_{-\omega_{max}}^{\omega_{max}} |H_{act}(\mathrm{j}\omega; \beta, \eta)|^2 \, \mathrm{d}\omega \right)^{1/2}. \tag{41}$$

The minimum of the output norm as a function of the balancing parameter β and of the loss parameter η is obtained by the following zero gradient conditions:

$$\frac{\partial \| V_{out}(\omega_{max}; \beta, \eta) \|_2}{\partial(\beta, \eta)} = 0, \tag{42}$$

where the partial derivatives relative to β and η are computed as

$$\frac{\partial \| V_{out} \|_2}{\partial(\beta, \eta)} = \frac{1}{2 \| V_{out} \|_2} \frac{1}{2\pi} \int_{-\omega_{max}}^{\omega_{max}} \frac{\partial |H_{act}|^2}{\partial(\beta, \eta)} \mathrm{d}\omega$$

$$= \frac{1}{2 \| V_{out} \|_2} \frac{1}{2\pi} \int_{-\omega_{max}}^{\omega_{max}} \left(\frac{\partial \operatorname{Re}^2(H_{act})}{\partial(\beta, \eta)} + \frac{\partial \operatorname{Im}^2(H_{act})}{\partial(\beta, \eta)} \right) \mathrm{d}\omega. \tag{43}$$

The real and imaginary parts of system transfer function H_{act} are computed for $s = \mathrm{j}\omega$ from equation (16) in the case of undamped mechanical system

$$\operatorname{Re}(H_{act}) = \eta, \qquad \operatorname{Im}(H_{act}) = \omega R_p C_p \beta - \omega R_p \sum_{i=1}^{+\infty} \frac{\theta_i^2}{m_i(\omega^2 + \omega_i^2)} \tag{44, 45}$$

and

$$\frac{\partial \operatorname{Re}^2(H_{act})}{\partial \beta} = 0, \qquad \frac{\partial \operatorname{Im}^2(H_{act})}{\partial \beta} = 2 \operatorname{Im}(H_{act}) \omega R_p C_p, \tag{46, 47}$$

$$\frac{\partial \operatorname{Re}^2(H_{act})}{\partial \eta} = 2\eta, \qquad \frac{\partial \operatorname{Im}^2(H_{act})}{\partial \eta} = 0. \tag{48, 49}$$

Substituting in equation (43)

$$\frac{\partial \| V_{out} \|_2}{\partial \beta} = \frac{1}{2 \| V_{out} \|_2} \frac{1}{\pi} \left\{ \frac{2}{3} \omega_{max}^3 (R_p C_p)^2 \beta - R_p \sum_{i=1}^{+\infty} \frac{\theta_i^2}{m_i} \left[\frac{\omega_i}{2} \log \left(\frac{\omega_i + \omega_{max}}{\omega_i - \omega_{max}} \right)^2 - 2\omega_{max} \right] \right\}, \tag{50}$$

$$\frac{\partial \| V_{out} \|_2}{\partial \eta} = \frac{1}{\| V_{out} \|_2} \frac{1}{\pi} \eta \omega_{max}. \tag{51}$$

In the limit case where the system input has unlimited bandwidth ($\omega_{max} \to \infty$), the first partial derivative simplifies to the purely electrical contribution

$$\frac{\partial \| V_{out} \|_2}{\partial \beta} = \frac{1}{2 \| V_{out} \|_2} \frac{1}{\pi} \left[\frac{2}{3} \omega_{max}^3 (R_p C_p)^2 \beta \right] \tag{52}$$

and the minimum condition is found for $\beta = \eta = 0$, i.e., when the readout bridge is electrically balanced and loss compensated.

6.1. PHYSICAL IMPLEMENTATION

As already mentioned, the correspondence of minimal output signal and electrical balancing and loss compensation can be expolited to tune the readout bridge. In practice, a tuning procedure is always necessary to cope with the non-negligible uncertainty and variability affecting the electrical parameters of the piezoelectric transducer.

In the case of manual tuning, a constant amplitude sweep is often adopted to drive the input. Resistances R_r and R_{lr} are the knobs to be used to make the β and η parameters null.

The tuning procedure can be automized adopting a standard self-tuning scheme based on the least-mean-squares (LMS) minimization of the bridge output signal (Figure 17).

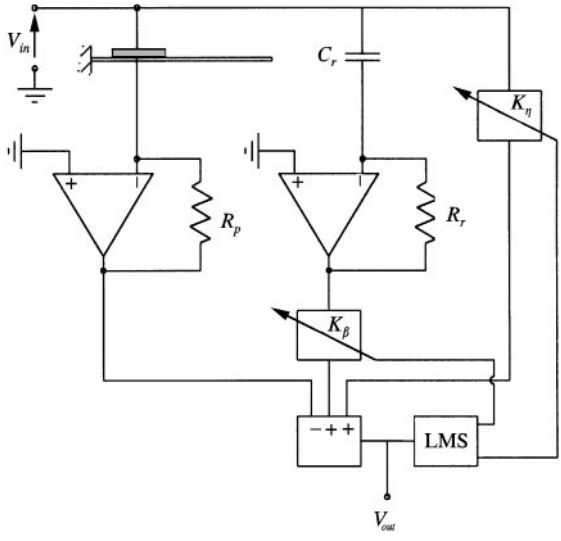

Figure 17. Piezoelectric self-sensing configuration: self-tuning readout bridge.

Remark 6. The order of the filter to be tuned must be limited to the first order to comply with the model of the electrical contribution of the piezoelectric admittance. In fact, the aim of the self-tuned arm of the bridge is to get rid of the electrical contribution (direct link) to the output signal, the mechanical contribution being the desired output of the self-sensing configuration of the piezoelectric transducer.

7. CONCLUSIONS

The behaviour of a structure equipped with a single piezoelectric transducer has been described in terms of its electromechanical admittance. This approach has enabled the study of different aspects of the use of the piezoelectric devices in a self-sensing context within a single consistent framework. The active and passive versions of the readout bridge have been compared, and the resulting system properties have been studied as a function of the relevant balancing parameters.

It has been shown that the poles structure is different for passive and active readout bridges and, significantly, does not depend on the bridge parameters for the latter. On the other hand, the zeros structure is common to both configurations and strongly depends on the bridge parameters and, in particular, on the balancing condition and on the compensation of the losses. The migration of the zeros as a function of the balancing parameter has been thoroughly described showing the possibility of non-minimum phase behaviour of the self-sensing system.

The effects of different reduction techniques have been studied and have been shown to be essential for the correct assessment of the balancing condition.

The extension of the analysis to the case of structures equipped with multiple self-sensing piezoelectric transducers is currently under study.

REFERENCES

1. J. Dosch, D. Inman and E. Garcia 1992 *Journal of Intelligent Material Systems and Structures* **3**, 166–185. A self-sensing piezoelectric actuator for collocated control.

2. E. ANDERSON and N. HAGOOD 1994 *Journal of Sound and Vibration* **174**, 617–639. Simultaneous piezoelectric sensing/actuation: analysis and application to controlled structures.
3. S. YANG and C. JENG 1996 *Journal of Smart Materials and Structures* **5**, 806–813. Structural vibration suppression by concurren piezoelectric sensor and actuator.
4. R. CLARK, W. SAUNDERS and G. GIBBS 1998 *Adaptive Structures—Dynamics and Control*. New York: Wiley.
5. E. BRUSA, S. CARABELLI and A. TONOLI 1998 *Proceedings of 5th Annual International Symposium on Smart Structures and Materials*, Vol. **3329**, 802–811. San Diego, U.S.A.: SPIE. Modeling and testing of plate structures using self-sensing piezoelectric transducers.
6. E. BRUSA, S. CARABELLI, F. CARRARO and A. TONOLI 1998 *Journal of Intelligent Material Systems and Structures* **9**, 198–209. Electromechanical tuning of self-sensing piezoelectric transducers.
7. Y. MIYAHARA, T. FUJII, S. WATANABE, A. TONOLI, S. CARABELLI, H. YAMADA and H. BLEULER *Applied Surface Science* **140**, 428–431. Lead Zirconate titanate cantilever for noncontact atomic force microscopy.
8. Y. MIYAHARA, T. FUJII, S. WATANABE, A. TONOLI, S. CARABELLI, H. YAMADA and H. BLEULER 1998 *Proceedings of the 1st International Workshop on Noncontact Atomic Force Microscopy*. Noncontact mode atomic force microscopy using piezoelectric cantilever.
9. D. MIU 1993 *Mechatronics*. New York: Springer-Verlag.
10. R. CANNON and D. ROSENTHAL 1984 *American Institute of Aeronautics and Astronautics Journal of Guidance* **7**, 546–553. Experiments in control of flexible structures with noncolocated sensors and actuators.
11. C. GOH and T. CAUGHEY 1985 *International Journal of Control* **41**, 787–802. On the stability problem caused by finite actuator dynamics in the collocated control of large space structures.
12. N. HAGOOD, W. CHUNG and A. V. FLOTOW 1990 *Journal of Intelligent Material Systems and Structures* **4**, 327–353. Modelling of piezoelectric actuator dynamics for active structural control.
13. E. BRUSA, S. CARABELLI and A. TONOLI 1996 *Proceedings of 7th International Conference on Adaptive Structures and Technology*, *Rome*, *Italy*. Self-sensing colocated structures with distributed piezoelectric transducers.
14. E. BRUSA, S. CARABELLI, F. CARRARO and A. TONOLI 1997 *Proceedings of 3rd Army Research Office Workshop*, *Blacksburg*, *Virginia*, *USA*. Electromechanical tuning of self-sensing piezoelectric transducers.

APPENDIX A: TEST RIGS

A.1. BEAM

The beam test set-up of Figure 3 is made of AISI 2024 aluminium alloy, 249 mm long, 32 mm wide and 1·6 mm thick. A PCE5 square piezoceramic transducer, 30 mm wide and 0·3 mm thick, is surface bonded 18 mm from the clamped section. A 0·1 mm thick kapton film is included in the bonding layer between the aluminium beam and the piezoelectric transducer to avoid the risk of short circuit between them, regardless of the connection of the piezoelectric.

With reference to the symbols adopted in equation (24), the main characteristics of the dynamic model of the beam are reported in Table 3 as a function of the corresponding mode. The modal natural frequencies ω_i have been measured with the piezoelectric short circuited. The modal damping factors ζ_i and the piezoelectric constants θ_i have been identified from the transfer functions of the self-sensing transducer obtained from a finite element model and the same transfer function measured during experimental tests.

As far as the electrical connection of the piezoelectric transducer is concerned, its upper electrode is connected to the output of the power amplifier, and the lower electrode to the current sensing device, as shown in Figures 1 and 2.

The electrical parameters of the transducer C_p^* and R_{lp} measured with an impedance meter are reported in Table 4 in the frequency range of the first and of the second mode. As the impedance measurement has been performed on the transducer installed on the beam,

TABLE 3

Modal parameters of the beam test rig

Mode no.	ω_i(Hz)	ζ_i(%)	θ_i (C/s^2 V)
1	20·8	0·1	$-3{\cdot}6\times10^{-3}$
2	122·4	0·3	$2{\cdot}7\times10^{-3}$
3	332·5	0·2	$-2{\cdot}5\times10^{-3}$
4	650·3	0·2	$1{\cdot}0\times10^{-1}$
5	1087	0·2	$-6{\cdot}8\times10^{-2}$

TABLE 4

Electrical parameters of the piezoelectric and of the other components of bridge circuit measured with an impedance meter. A voltage amplitude of 100 *mV has been adopted as excitation of the piezoelectric device and reference capacitance during the impedance measurement*

Frequency range	10–100 Hz	100–350 Hz
C_p^* (nF)	27·5	26·8
R_{lp} (MΩ)	10·9	2·7
R_p (kΩ)	10·0	10·0
C_r (nF)	27·5	27·5
R_{lr} (MΩ)	10·8	2·6
R_r (kΩ)	10·1	9·5

the measured values include both the electrical and mechanical contributions of equation (25). The values of resistances R_p, R_r and R_{lr} adopted to balance the bridge in the same frequency ranges are reported in the same Table 4.

A.2. PLATE

The plate test set-up of Figure 4 is made of AISI 2024 aluminium alloy, 400 mm × 450 mm wide and 1 mm thick. The plate is clamped on all its sides to a 45 kg mass steel base plate which is used as a seismic mass. Four rubber silent blocks are used to support the base plate on the floor of the laboratory. Six PCE5 rectangular piezoceramic transducers 30 mm × 20 mm wide and 0·5 mm thick are bonded on the upper surface of the plate using the same kapton film adopted for the beam structure, to isolate the electrode to the plate that is electrically grounded. The location of the piezoelectric transducers has been chosen to maximize interaction with the first four bending modes of the plate as describe in reference [14].

Each transducer is connected to a couple of dedicated electric terminals to be driven individually. These terminals are left electrically floating to ensure the inclusion of each transducer in self-sensing bridge readout circuits. The experimental results of Figures 14 and 16 are obtained by the connection of piezoelectric transducers 1, 3, 4, and 6 to the same electrical node; the connection is made so that transducers 1 and 3 are subject to the same

TABLE 5

Modal parameters of the plate test rig

Mode no.	ω_i(Hz)	ζ_i(%)	θ_i (C/s^2 V)
1	50·4	0·3	0
2	115	0·5	0
3	121	0·4	0
4	165	1·1	$2{\cdot}1 \times 10^{-2}$
5	188	1·0	0
6	230	1·0	0

TABLE 6

Electrical parameters of the modal transducer formed by piezoelectric transducers 1, 3, 4, 6 *measured with an impedance meter. A voltage amplitude of* 100 *mV has been adopted as excitation of the piezoelectric device and reference capacitance during the impedance measurement*

Frequency range	100–300 Hz
C_p^* (nF)	46·3
R_{lp} (MΩ)	1·3
R_p (kΩ)	10·5
C_r (nF)	47·0
R_{lr} (MΩ)	1·3
R_r (kΩ)	10·6

electrical field relative to their polarization while transducers are connected with reversed polarity relative to transducers 1 and 3. Transducers 2 and 5 are left open circuited. This connection of transducers 1, 3, 4, and 6 makes them behave as a single transducer which approximates to a modal transducer acting on the fourth flexural mode of the plate.

The main characteristics of the dynamic model of the plate are reported in Table 5 as a function of the corresponding mode. The value of electromechanical model coefficients θ_i are obtained from the finite element model of the plate and are relative to the adopted connection scheme. Modal coefficient θ_4 has then been identified by comparing the system transfer function obtained from the finite element model to the measured one. The reported natural frequencies and modal dampings have been measured with short-circuited piezoelectric transducers.

The electrical parameters of the transducer C_p^* and R_{lp} measured with an impedance meter are reported in Table 6 in the frequency range of the fourth mode. Similar to the case of the beam the measured capacitance value includes both the electrical and mechanical contributions. The values of resistances R_p, R_r and R_{lr} adopted to balance the bridge in the same frequency ranges are reported in Table 6.